Atmos. Meas. Tech., 7, 1999–2012, 2014
www.atmos-meas-tech.net/7/1999/2014/
doi:10.5194/amt-7-1999-2014

Atmospheric Measurement Techniques
Open Access

Improving accuracy and precision of ice core $\delta D(CH_4)$ analyses using methane pre-pyrolysis and hydrogen post-pyrolysis trapping and subsequent chromatographic separation

M. Bock, J. Schmitt, J. Beck, R. Schneider, and H. Fischer

Climate and Environmental Physics, Physics Institute and Oeschger Centre for Climate Change Research, University of Bern, Sidlerstrasse 5, 3012 Bern, Switzerland

Correspondence to: M. Bock (bock@climate.unibe.ch)

Received: 28 November 2013 – Published in Atmos. Meas. Tech. Discuss.: 19 December 2013
Revised: 20 May 2014 – Accepted: 28 May 2014 – Published: 4 July 2014

Abstract. Firn and polar ice cores offer the only direct palaeoatmospheric archive. Analyses of past greenhouse gas concentrations and their isotopic compositions in air bubbles in the ice can help to constrain changes in global biogeochemical cycles in the past. For the analysis of the hydrogen isotopic composition of methane ($\delta D(CH_4)$ or $\delta^2H(CH_4)$) 0.5 to 1.5 kg of ice was hitherto used. Here we present a method to improve precision and reduce the sample amount for $\delta D(CH_4)$ measurements in (ice core) air. Preconcentrated methane is focused in front of a high temperature oven (pre-pyrolysis trapping), and molecular hydrogen formed by pyrolysis is trapped afterwards (post-pyrolysis trapping), both on a carbon-PLOT capillary at −196 °C. Argon, oxygen, nitrogen, carbon monoxide, unpyrolysed methane and krypton are trapped together with H_2 and must be separated using a second short, cooled chromatographic column to ensure accurate results. Pre- and post-pyrolysis trapping largely removes the isotopic fractionation induced during chromatographic separation and results in a narrow peak in the mass spectrometer. Air standards can be measured with a precision better than 1 ‰. For polar ice samples from glacial periods, we estimate a precision of 2.3 ‰ for 350 g of ice (or roughly 30 mL – at standard temperature and pressure (STP) – of air) with 350 ppb of methane. This corresponds to recent tropospheric air samples (about 1900 ppb CH_4) of about 6 mL (STP) or about 500 pmol of pure CH_4.

1 Introduction

Methane (CH_4) is a potent greenhouse gas, which shows increased atmospheric concentrations since the industrial revolution (Intergovernmental Panel on Climate Change, 2007). A recent assessment of the present-day methane budget is presented in Kirschke et al. (2013). However, the atmospheric load of CH_4 has varied on various timescales. A wealth of information has been gained from concentration measurements regarding annual (Dlugokencky et al., 1995), decadal (Mitchell et al., 2011), and millennial up to glacial–interglacial (Loulergue et al., 2008) CH_4 variability. Stable isotope data of methane on recent air samples (e.g. Quay et al., 1999) and on the past atmosphere using ice cores (e.g. Ferretti et al., 2005; Fischer et al., 2008; Sowers, 2010; Sapart et al., 2012; Möller et al., 2013) provide further insight into processes and sources controlling the global methane cycle. For instance, knowledge of the temporal evolution of the hydrogen isotopic composition of methane ($\delta D(CH_4)$ or $\delta^2H(CH_4)$) over the termination of the last ice age (14 000–18 000 years before present) (Sowers, 2006) as well as during rapid warming events between 32 000–42 000 years before present (Bock et al., 2010b) made it possible to reject the "clathrate gun hypothesis" proposed by Kennett et al. (2003) as the trigger for the steep atmospheric methane increases.

However, we are still far from a complete picture of the biogeochemistry of methane in the past. Ice core isotope studies on $\delta D(CH_4)$ have the potential to improve our understanding of the global CH_4 cycle but are still scarce due to analytical difficulties (e.g. Bock et al., 2010a; Sapart et al., 2011) and the large sample amount needed. To date, the

few published ice core δD(CH_4) studies required from 0.5 kg (Bock et al., 2010b) to more than 1 kg (Sowers, 2006, 2010; Mischler et al., 2009) of ice from multi-parameter deep ice cores with a typical precision of around 3 to 4 ‰. This error bar is still large in view of the observed natural variability, which is rather small: about 30 ‰ for glacial–interglacial and 20 ‰ for rapid changes during the last glacial (Sowers, 2006; Bock et al., 2010b). This study presents new developments based on Bock et al. (2010a) to improve precision and accuracy and significantly reduce the sample size for (ice core) δD(CH_4) measurements.

2 Experimental

We present an improved continuous-flow gas chromatography (GC) pyrolysis (P) isotope-ratio monitoring mass spectrometry (irmMS) system (GC/P/irmMS) designed to analyze δD(CH_4) from (ice core) air samples (Fig. 1) with high precision. In the following we give a short summary of our previous instrumentation (Bock et al., 2010a) and new developments concerning the physical system and data processing.

The most important new features presented here are pre- and post-pyrolysis trapping (pre&postPT) of CH_4 and molecular hydrogen (H_2), respectively, and subsequent gas chromatographic separation using a cooled porous layer open tubular (PLOT) column, which improve accuracy and precision and reduce the required sample amount considerably. A systematic dependency of δD(CH_4) on the amount of CH_4 (signal dependency) is observed but can be precisely corrected for. The successful implementation of pre&postPT requires as a prerequisite better purification of helium. A new calibration software tool has also been developed, enabling a one-step correction of system drifts over time and signal dependency (linearity) in an iterative way.

Note that the current status of our set-up has been reached in separate steps over the last few years. The different states are summarized in Table 1 and Fig. 1, named after the year(s) and depicted in different colours. Until 2010 no pre&postPT and subsequent gas chromatographic separation was performed. In the years 2011 and 2012, we took advantage of post-pyrolysis trapping and basic GC separation afterwards. In 2013 we also implemented pre-pyrolysis trapping but still used the same basic second GC. Furthermore, since the beginning of 2014 an enhanced, cooled 2nd GC is additionally operated.

2.1 Instrumentation

The system is fed by helium (He) (Alphagaz I, 99.9990 % purity; Carbagas, Switzerland), which is purified using a high-capacity gas purifier and an inline gas purifier (both Supelco, Bellefonte, PA, USA). In addition to the description given by Bock et al. (2010a), we further purify the He used for the complete system in a 3 m long 1/4 in. stainless steel (SST) capillary (i.d. 5.3 mm) filled with charcoal (grain size 0.3–0.5 mm, 0.41 g cm^{-3}, Fluka 05112; Sigma-Aldrich Chemie, Steinheim, Germany). This trap is immersed in liquid nitrogen (LN) during the week and can be vented at room temperature over the weekend using valve V0 in Fig. 1, a pneumatic six-port, two-position valve (1/16 in. fittings, 0.4 mm port diameter, Valcon M rotor; Valco, VICI AG, Schenkon, Switzerland). The additional He purification cold trap lowers the blank CH_4 contribution considerably compared to Bock et al. (2010a). Extracting remnant gas in the sample cylinder (containing melt water) after an ice sample results in an H_2 peak 0.5 % the area of a small CH_4 peak characteristic for the LGM (Last Glacial Maximum – CH_4 concentration of 350 ppb – about 20 ka before present (BP), where present is defined as 1950; Loulergue et al., 2008; Clark et al., 2009). In comparison, the same procedure in the old system led to a 1 % area of a LGM peak; thus, blank CH_4 contribution appears to be reduced by 50 % for the improved set-up. To factor out the blank contribution from the extracted sample and, for example, the sample cylinder walls, we trapped background gases (from the He carrier gas) on T2, thus bypassing the sample cylinder, which resulted in a peak area of only 0.2 %.

The following sample preparation steps are similar to Bock et al. (2010a): a glass vessel containing an ice core sample is evacuated, and the enclosed air is released upon melting the ice. In a high flow (He, 500 mL min^{-1}), water vapour is removed using a cooled Nafion membrane and a cold trap (T1) while the air sample is transferred to a trap filled with charcoal (T2) immersed in LN.

Contrary to Bock et al. (2010a), T1 is made up of an empty 1/8 in. tube of three coils that enter or leave a dewar maintained at −90 °C. Temperature controlled cooling of the dewar is achieved using LN droplets released into the dewar (Schmitt, 2006; Bock et al., 2010a). Only residual water vapour is removed by T1, while CO_2 is adsorbed on an Ascarite trap beforehand, made of a 10 cm 1/4 in. stainless steel tube. In this new set-up, N_2O is passed through the system and can be measured in the mass spectrometer.

Air reference injections are realized by switching V1, either mimicking an ice sample by introducing the air into the glass extraction vessel or by bypassing the sample vessel, depending on the position of V2. Following a switch of V3, the air sample is transferred from the charcoal trap to a trap filled with Hayesep D (T3, at −100 °C), where methane is quantitatively trapped while the bulk air (N_2, O_2, Ar) is vented. Residual air components and CH_4 are focussed on T4 (three coils of a GC column (CP-PoraBond Q, 0.32 mm i.d.) at −196 °C) and injected onto a GC column (Carboxene 1010 PLOT column (30 m, i.d. = 0.32 mm)). Valve V5 is switched to route the sample through a new cold trap T5 and towards the pyrolysis furnace only for the time window in which CH_4 is leaving the GC column. T5 replaces Nafion-2 of the old set-up, which was less effective in removing water before the pre- and post-pyrolysis trapping steps, and consists of a

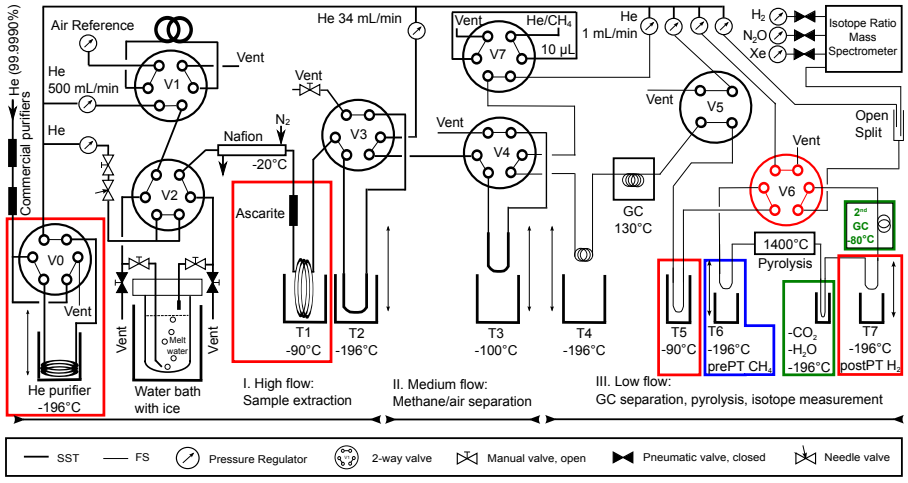

Figure 1. Flow scheme of the new δD(CH_4) system including pre- and post-pyrolysis trapping of methane and hydrogen, respectively, and a second short, cooled chromatographic separation column (2nd GC) after the last trap. The coloured boxes highlight the major differences compared to Bock et al. (2010a). Red are the changes made in 2011–2012, blue represents additional changes carried out in 2013 and green in 2014 (compare Table 1). Capillaries are stainless steel (SST) or fused silica (FS), with the latter occurring only in the low-flow part. Inside the GC we use a Carboxene 1010 PLOT column (30 m, i.d. = 0.32 mm). Cold traps are "He purifier" (charcoal, 1/4 in.), T1 (open tube, 1/8 in.), T2 (charcoal, 1/4 in.), T3 (Hayesep D, 1/8 in.), T4 (CP-PoraBond Q, i.d. = 0.32 mm), T5 (open untreated capillary, i.d. = 0.53 mm), T6, T7 and 2nd GC (all GS-CarbonPLOT, i.d. = 0.32 mm). The CO_2 and H_2O trap after the pyrolysis oven consists of a piece of untreated capillary (i.d. 0.32 mm) immersed in LN.

U-shaped piece of untreated capillary (i.d. = 0.53 mm) placed in a well-insulated dewar cooled by LN droplets to −90 °C.

In the following we describe the main new developments. Eluting CH_4 from the GC is focused on T6 for 18 s (pre-pyrolysis trapping, prePT) before it is released by passive warming to room temperature. Subsequently, the focussed pulse of CH_4 is pyrolysed as described by Bock et al. (2010a), but the produced H_2 and the pyrolysis side products are not allowed to enter the mass spectrometer (Isoprime, Elementar Analysensysteme, Hanau, Germany) directly. Instead, the pyrolysis products are trapped on T7 for 40 s (post-pyrolysis trapping, postPT). Both traps – T6 and T7 – are U-shaped, 20 cm long GC columns (GS-CarbonPLOT, ID 0.32 mm, film 1.5 µm, Agilent Technologies, part number 113-3112) retaining CH_4 and H_2 (and other gases) at LN temperature. After postPT is complete, T7 is lifted out of LN and warmed to room temperature allowing H_2 to enter the mass spectrometer via an open split. After T7 the line has been extended by two meters of the same PLOT column (2nd GC in Fig. 1), of which 70 cm are cooled to −80 °C to ensure baseline separation of H_2 from other gases, which produce signals visible in both the m/z 2 and 3 traces (Fig. 2). The column piece of the 2nd GC is cooled on a well insulated brass surface by two thermoelectric coolers/heaters (20 W, 25 g, PKE 36 A 001, Peltron GmbH, Fürth, Germany) with the heat sink (a copper plate) immersed in LN. Temperature is controlled by a thermostat (Jumo) to within 0.5 °C and can be set in a dynamic range of −70 to −100 °C. To prevent CO_2 and H_2O (eluting from the pyrolysis oven) from accumulating on the cold 2nd GC column, a short piece of untreated fused silica capillary is immersed in LN during the day. Valve V6 is used to bypass the pyrolysis furnace, traps T6 and T7, the CO_2 and H_2O trap, and the 2nd GC in order to vent water eluting from a warm T5 trap.

Note that in an earlier version, our system was only extended by post-pyrolysis trapping, while pre-pyrolysis trapping was implemented later (Table 1 and Fig. 1). The latter is of potential interest as CH_4 and CDH_3 experience different retention on GC columns (e.g. Bock et al., 2010a), leading to a "time shift" (Ricci et al., 1994) or "time displacement" (Meier-Augenstein, 1999). As both CH_4 and CDH_3 are held on T6, this pre-pyrolysis trapping step resets the chromatographic separation introduced by the GC, allowing for pyrolysis of a non-fractionated methane peak. Furthermore, prePT allows for a shorter post-pyrolysis trapping time, as H_2 from CH_4 pyrolysis elutes during a shorter time interval. This is advantageous because H_2 cannot be held on T7 for an extended time under the described conditions. Instead, strong chromatographic separation between H_2 and HD for a system using a long post-pyrolysis trapping time leads to strong intra-peak fractionation visible in a large time shift.

Pyrolysis of CH_4 is achieved using a custom-made high-temperature furnace (Bock et al., 2010a). Using a brand new thermocouple indicated that the optimal pyrolysis temperature in our case is 1400 °C. However, due to ageing of the thermocouple, the read-out of the temperature is considerably reduced over a time period of several months. To determine the optimal pyrolysis temperature, we introduce

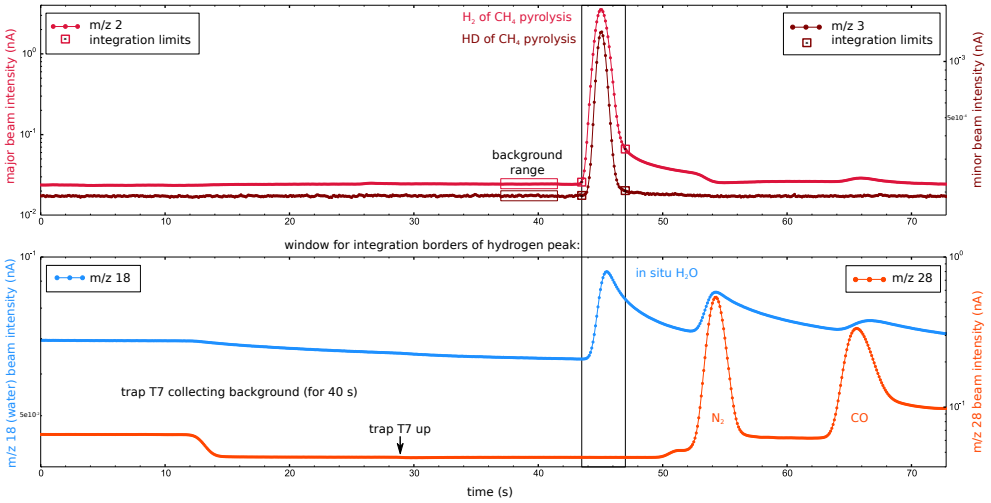

Figure 2. Chromatogram of signals induced by a pure CH_4 in He injection on logarithmic scales. Note that each beam is on its own scale. The top panel shows the hydrogen peak on m/z 2 and 3. The bottom panel displays the signals measured when the mass spectrometer is focussed to either m/z 18 (water) or m/z 28 (N_2 and CO). Clearly, N_2 and CO, which are trapped together with H_2 on T7, are well separated from H_2 by our cooled 2nd GC. A signal on m/z 18 (and 17, water), which is produced in situ in the mass spectrometer, is visible for H_2, but also for N_2 and CO (compare text and Table 2). Individual backgrounds of the measured signals of 0.8, 0.0015, 0.2 and 0.2 nA are subtracted for beams of m/z 2, 3, 18 and 28, respectively.

CH_4 peaks via V7 (e.g. 3 times 10 µL loop with roughly 500 ppb CH_4 in He) at different temperatures. We observe two plateaus at different temperatures, one for δD(CH_4) values and one for peak areas. The plateau of δD(CH_4) at higher temperature is favoured for high-precision isotope measurements because the small but inevitable temperature fluctuations in the reactor then lead to smaller scatter in isotope values. Too high temperatures lead to shortened lifetimes of pyrolysis reactors which becomes noticeable through higher backgrounds of nitrogen and argon caused by ambient air. Typically, a reactor (stone-ware GmbH, Switzerland, DEGUSSIT® Al_2O_3, length = 420 mm, i.d. = 0.5 mm, o.d. = 1.5 mm) facilitates reproducible results for about half a year. When a new reactor has to be installed, it is heated up using a ramp of 5 h and pre-conditioned over the course of a day by injecting 10 µL loops of the previously mentioned mixture of 500 ppb CH_4 in He every 40 s (without using any trap).

As a second major improvement to the system following a development by Schmitt et al. (2014), we can now measure N_2O concentration, δ^{15}N and δ^{18}O of N_2O on the same sample. Therefore, after the H_2 acquisition for methane is completed, the pyrolysis reactor is bypassed using valve V6 and a peak jump is performed in order to focus the mass spectrometer to the N_2O configuration measuring m/z 44, 45, and 46. After a second peak jump, we measure xenon (as $^{132}Xe^{2+}$ and $^{136}Xe^{2+}$) using beams m/z 66 and 68. Xenon is considered a proxy for total air content and is used to calculate CH_4 and N_2O concentrations. For detailed descriptions of N_2O and Xe analytics, we refer the reader to a companion publication by Schmitt et al. (2014) reporting on a new system to simultaneously measure $\delta^{13}CH_4$, isotopes of N_2O, Xe and more trace gas concentrations.

2.2 Data processing

We use custom-made Python (http://www.python.org/) scripts to process the raw beam data, to organise peak data of references, standards and samples in specific libraries and to perform the calibration to the international VSMOW (Vienna standard mean ocean water) scale. The peak integration method is similar to that described by Bock et al. (2010a). Integration limits are found based on the major beam time series and also applied to the minor beam. In commercially available mass spectrometer software, the integration limits are determined based on the derivative of the beam time series according to thresholds of the slope (e.g. Ricci et al., 1994). We chose a different approach here: we determine the peak maximum and set the integration limits to fixed numbers of data points before and after the peak maximum, that is, we use a fixed peak width. This choice is not critical as an alternative peak evaluation using the commonly used start- and end-slope criteria (Ricci et al., 1994) led to the same results within the given error limits (re-evaluated data not shown). In contrast to our previous procedure, pre&postPT removes the isotopic fractionation induced by the chromatographic separation resulting in nearly unfractionated H_2 peaks in the current set-up. Hence, we do not perform a time shift correction of the m/z 3 beam. Generally, the background is determined as the median of data points 6 s before the peak start (see Fig. 2).

Table 1. Time line of our measurement system. Shown are the key properties of the system that changed over the course of the past four years. Colours refer to successive changes indicated in Fig. 1 and are in line with Fig. 4.

Name	2010	2011–2012	2013	2014
colour	black & white	red	blue	green
Reference	Bock et al. (2010)	Bock et al. (2013)	Bock et al. (2013)	this study
Short description	GC-pyrolysis-IRMS	Post-pyrolysis trapping, basic 2nd GC separation afterwards	Pre- & post-pyrolysis trapping, basic 2nd GC separation afterwards	Pre-& post-pyrolysis trapping, enhanced 2nd GC separation afterwards
Key property	All mentioned substances interfere with H_2	Separation of unpyrolysed CH_4 and Kr from H_2	As 2011–2012 plus pyrolysis of non-fractionated CH_4 and measurement of non-fractionated H_2 peak	As 2013 plus H_2 peak free of known interferences (except unavoidable H_2O formed in situ in ion source)

In order to calibrate samples, it is essential to compare samples to reference measurements that are sufficiently stable over time and match the sample size. If this cannot be achieved, one has to correct for any drift and signal dependency (e.g. Schmitt et al., 2003; Potter and Siemann, 2004; Bock et al., 2010a; Brass and Röckmann, 2010). In our case this is essential, because we observe a clear signal dependency of the δD(CH_4) values (Fig. 3a). We note that the H_3^+ factor did not change compared to Bock et al. (2010a) and is accounted for during evaluation of chromatograms. Hence, residual signal dependency is due to processes upstream of the mass spectrometer (e.g. pyrolysis conditions). The observed signal dependency is stable and reproducible over long time intervals and can therefore be precisely corrected for without compromising the overall precision of the measurement (see Sect. 3.2). When a new pyrolysis reactor is installed, the signal dependency may change, and a new interval of our data analysis has to be started to account for this change. We developed a new software routine to correct for any system (time) drift and signal dependency simultaneously; this is presented in detail in the Appendix of this article and Fig. 3a and b. It takes standard measurements of known isotopic signature and iteratively fits parameters for (temporal) drift and signal dependency at the same time in order to minimize the standard deviation of δD(CH_4) of this reference air. The latter assumes constant signal dependency within a certain time period (typically a few weeks). The same assumption holds for laboratories determining signal dependency on a periodic schedule, but we see two advantages of our approach: (1) no extra day is needed to examine signal dependency and (2) if signal dependency changes slightly during the chosen time interval, this change is already accounted for by our reference measurements covering this interval. The fit parameters and daily mean values of our reference "Air Controlé" are used to calibrate the samples.

3 System performance

3.1 Accuracy

Our reference used to calibrate all samples is Air Controlé, a recent clean air tank (CH_4 concentration = [CH_4] = 1971 ± 7 ppb) for medical purposes (bottle 541659, filled February 2007 in Basel, Switzerland, Carbagas). Air Controlé was cross-referenced to −93.6 ‰ with respect to Vienna standard mean ocean water (VSMOW) using bottled air from Alert station "Alert 2002/11" (Bock et al., 2010a; Poss, 2003; Marik, 1998), previously measured at the Institute of Environmental Physics in Heidelberg (IUP, University of Heidelberg, Germany). At the IUP two scales for δD(CH_4) co-exist; one is based on mass spectrometric measurements of water-derived H_2 (named MAT), and the other is based on methane-in-air gases measured using a tunable diode laser system (named TDLAS). The anchors

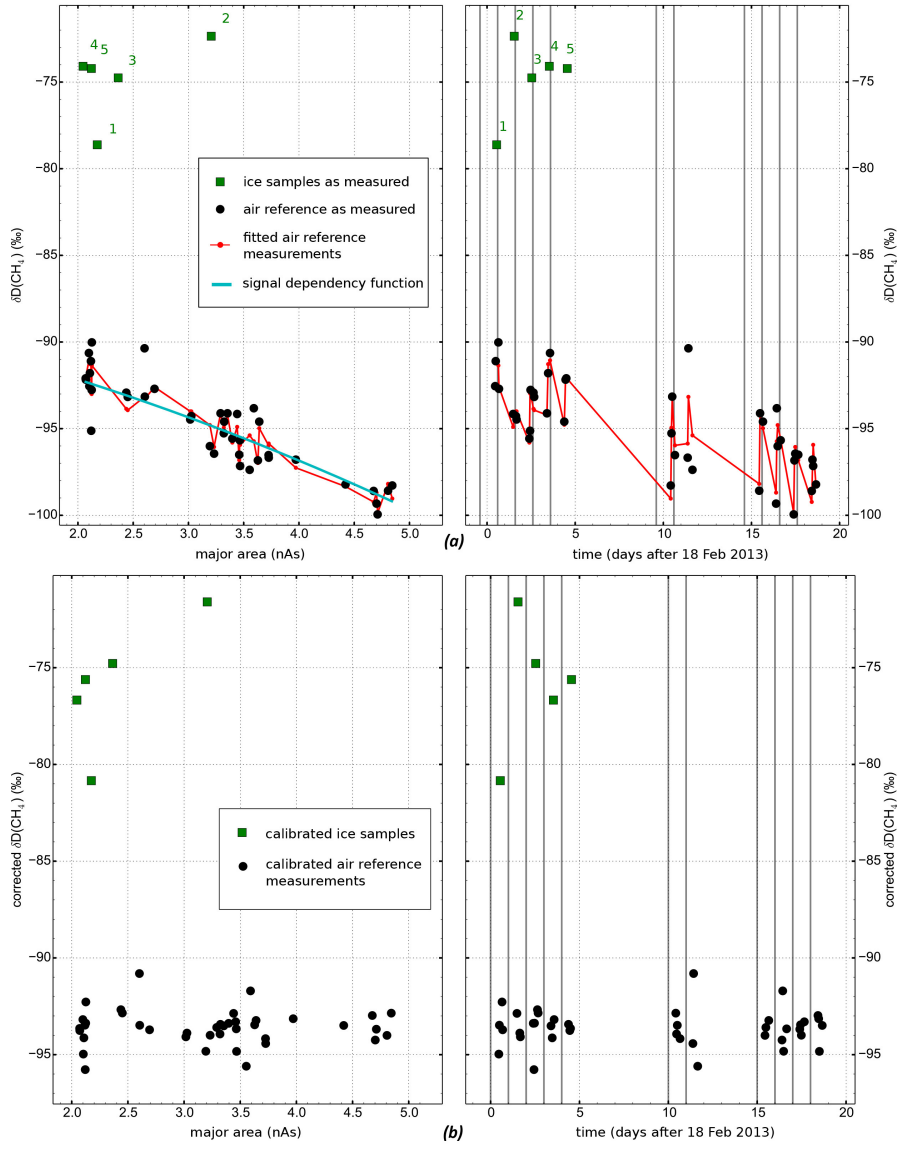

Figure 3. (a) Top panels: uncalibrated δD(CH$_4$) data of our reference Air Controlé (black bullets) and B34 ice core samples (green squares). The left panel shows δD(CH$_4$) vs. major area, i.e. the observed signal dependency including temporal drift. The right panel shows the same uncalibrated data set plotted against time. The red dots and line show the fitted standard numbers, which are later used to calibrate the samples, as described in the Appendix. The closer the red and black symbols are to each other, the better the fit. The cyan line indicates the polynomial correction function for signal dependency.
(b) Bottom panels: calibrated δD(CH$_4$) data of Fig. 3a after correction for temporal drift and signal dependency using the software described in the Appendix. The left panel shows δD(CH$_4$) vs. major area and the right panel shows the same calibrated data set plotted against time. Black bullets show standard measurements (Air Controlé); green squares show B34 ice core samples.

are IAEA (International Atomic Energy Agency) water standards VSMOW and VSLAP (Vienna standard light Antarctic precipitation) for MAT and CH$_4$ in air standards, the latter originally calibrated by the Bundesanstalt fuer Geowissenschaften und Rohstoffe (BGR) Hannover, Germany for TDLAS (Bergamaschi et al., 1994, 2000). The two scales agree within 1.0 ‰ (MAT > TDLAS), which is within their precisions of 2.4 ‰ and 1.0 ‰ for MAT and TDLAS, respectively. δD(CH$_4$) for Alert was measured in Heidelberg twice using each method and was calibrated with respect to the mean of both scales (-82.2 ‰ $\pm$ 1.0 ‰, C. Veidt, personal communication, 2014). Error propagation of the measurements performed in Heidelberg and Bern to get from primary standards to the value of Air Controlé, which we use to calibrate samples, leads to an uncertainty of 3.5 ‰.

In our previous report (Bock et al., 2010a), we presented 4 air samples (Dome 6, Dome 13, Groningen Air, NAT-332 air) in the δD(CH$_4$) interval [-70, -110 ‰] in good agreement

Table 2. Sequence of detected species using the 2014 set-up (Fig. 1 and Table 1). Retention time (RT) is given relative to the H_2 peak maximum. Ar, O_2 and N_2 are not well-separated from each other under the described conditions. For CH_4 and Kr, the start of peaks is given, as the two substances elute very broadly from the cooled PLOT column. H_2O does not enter the mass spectrometer but is produced in situ (see text).

Substance	RT (s)	Origin	Influence on target beams	Visible on beam(s)
H_2	0	pyrolysis-derived sample-CH_4	target (positive peak on both m/z 2 and 3)	m/z 2 and 3
Ar	9	collected background of low-flow part	negative signal on m/z 2 (none on m/z 3)	m/z 40
O_2				m/z 16, 32
N_2				m/z 14, 28 (44)
CO	20.4	CH_4 pyrolysis side product	positive signal on m/z 2 (none on m/z 3)	m/z 12, 16, 28 (44)
H_2O	0.5	in situ production in mass spectrometer	positive signal on m/z 2 (none on m/z 3)	m/z 16, 17, 18
	9.3			
	21.6			
CH_4	185	unpyrolysed sample CH_4	positive signal on m/z 3 (small on m/z 2)	m/z 15, 16
Kr	210	only from Kr containing air samples	positive signal on m/z 2, negative on m/z 3	m/z 43

with Bräunlich et al. (2001) and younger measurements performed by the Institute for Marine and Atmospheric research Utrecht (IMAU) (Sapart et al., 2011), who so far use the same TDLAS scale as IUP. Two of these air samples (at the margins of the δD(CH_4) interval) have been re-measured with our improved set-up (Table 1, Fig. 1), again with good agreement (Table 3). Note that a new independent scale for δD(CH_4) is currently being established at MPI for Biogeochemistry, Jena. Accordingly, stringent Round Robin tests for methane isotopes will make it possible to check the agreement of different δD(CH_4) scales in the future.

In summary, we are confident that our measurements are close to the VSMOW scale (to about 3.5 ‰); however, we note and will show later in this section that effects due to differences in matrix and/or concentration of samples and references can hamper highly accurate results, while deviations are difficult to pinpoint for individual laboratories and inter laboratory comparison exercises.

As an update from Bock et al. (2010a), we introduce a new standard gas here: "Saphir 4" (bottle 4405, Carbagas, artificial clean air mixture with 761 ppb CH_4 and no krypton). Saphir injections through the melt water of a previously extracted ice core sample are slightly depleted in deuterium (ca. 2 ‰, see Table 3) compared to Saphir injections bypassing the sample container, but the mean values are within the combined error. Taking the small difference at face value, this fits to our expectation of preferential dissolution of the heavy isotope in the denser medium. If the extraction efficiency is equal for CH_4 and CDH_3 (or less for the heavier isotopologue), we expect lighter values for air standard injections flowing through melt water. Unfortunately, we cannot quantify the process, as there is no ice sample with known isotopic composition of the occluded air. Note, that any bias would only be relevant for intercomparison exercises with other labs, but would not influence the interpretation of time series or interpolar difference studies consistently carried out with our set-up. To conclude, it is not clear whether the aforementioned offset prevails for ice samples, or if the effect only occurs after ice sample extractions. We therefore chose not to correct for this (potential but) insignificant offset.

Note that our results for WAIS (West Antarctic ice sheet, core WDC05A, tube 184, depth range: 172.74–173.03 m, age approximately 410 a BP) are 15 ‰ more enriched in deuterium compared to data presented in Mischler et al. (2009). This offset is similar to the one observed for Boulder air (Bock et al., 2010a) compared to measurements performed at the Stable Isotope Lab of the Institute of Arctic and Alpine Research (INSTAAR, University of Colorado, Boulder, CO, USA) and reflects the fact that the laboratories in the US and Europe are tied to different primary standard air bottles. Note that no internationally accepted isotope reference material for CH_4 from air samples is yet available. At the time of writing, the aforementioned lab offsets are being addressed in a Round Robin organized by T. Sowers and E. Brook using WAIS ice and bottled air samples with varying methane concentrations.

Post-pyrolysis trapping and subsequent gas chromatographic separation enables the measurement of a pure H_2 peak in the mass spectrometer. Recently Schmitt et al. (2013) demonstrated that krypton (Kr) interference is possible during carbon isotopic analyses of CH_4. Conventional stable isotope analysis of CH_4 using GC-IRMS without post-conversion separation leads to insufficient separation of CH_4 and Kr. In the case of $\delta^{13}CH_4$, the influence of Kr on $\delta^{13}C$ analysis leads to a significant alteration of the results. Similarly, Meier-Augenstein et al. (2009) reported interference of N_2 for H_2 analyses. In the discussion version of this contribution, we thoroughly demonstrate the influence of

Table 3. Results obtained with the new δD(CH_4) system (green boxes in Fig. 1) in comparison to our previous set-ups (Table 1). Mean values are given in column 3; columns 4 and 5 show standard deviations (1σ) of samples and Air Controlé reference air measurements, respectively. Air Controlé measurements are used to calibrate the samples to the international VSMOW scale. Air Controlé has been cross-referenced with respect to Alert (see text). The value given for Alert in the column for 2010 is given by C. Veidt (personal communication, 2014). "N" represents the number of measurements used: subscripts "SA" and "REF" in columns 2 and 6 denote sample and reference (i.e. Air Controlé), respectively. Columns 7–11 are arranged in the same pattern for the data with only basic GC separation after pre&postPT (Bock et al., 2013) (red and blue boxes in Fig. 1). Columns 12–14 show values obtained with the previous set-up presented in Bock et al. (2010a). Ice sample results are not corrected for any firn diffusion process. Gas ages of the ice samples are estimated as follows: B30 – 670 a BP, B34 – 1400 to 1530 a BP, and WAIS – 410 a BP. The WAIS samples are from core WDC05A, tube 184, depth range: 172.74–173.03 m. NGRIP gas samples date from between 870 and 9000 a BP.

	This study (green)					Bock et al. (2013) (blue)					Bock et al. (2010a)		
Sample description (sample size, origin CH_4 concentration)	N_{SA}	δD(CH_4) mean (‰)	1σ sample (‰)	1σ reference (‰)	N_{REF}	N_{SA}	δD(CH_4) mean (‰)	1σ sample (‰)	1σ reference (‰)	N_{REF}	N_{SA}	δD(CH_4) mean (‰)	1σ sample (‰)
Air reference and samples													
Alert ("2002/11", [CH_4] = 1831 ppb)	6	−81.4	0.5	0.6	21							−82.2	1.0
Air Controlé (all injections, 4–40 mL)	47	−93.6	1.1		47	544	−93.6	1.3		544	343	−93.6	2.8
Air Controlé (only larger loops (18–40 mL)	21	−93.6	0.6		21	69	−93.6	0.8		69	86	−93.5	2.3
Saphir 4 ([CH_4] = 761 ppb)	5	−169.6	1.5	1.1	26	36	−171.6	1.2	0.9	240			
Saphir 4 (loop after sample)	3	−171.6	1.1	1.1	26	34	−173.2	1.4	0.9	240			
Saphir 3 ([CH_4] = 1004 ppb)						2	−173.4	0.4	0.9	15	18	−167.6	2.4
Boulder (CAO8289 [CH_4] = 1500 ppb)	4	−81.2	0.5	0.6	21	14	−81.0	1.1	0.7	29	8	−80.8	1.3
NAT-332 ([CH_4] = 2141 ppb)	2	−107.7	1.1	0.5	12	3	−108.0	1.8	0.8	19	6	−106.3	1.2
Dome 6 (firn air [CH_4] = 1718 ppb)	2	−71.8	0.1	0.5	12	2	−71.0	0.8	0.2	8	2	−71.0	0.1
Ice core samples													
B30 (Greenland, pre-industrial, depth range 2 m)						2	−91.5	0.8	1.1	49	14	−94.7	−3.7
WAIS (Antarctica, pre-industrial, parallel replicates)						4	−73.0	0.5	1.2	20			
B34 (Antarctica, late Holocene, depth range 9 m)	4	−71.4	1.5	1.1	26	47	−74.6	2.8	1.5	422			

Ice core replicates	N_{SA}	depth intervals	pooled 1σ
B34 ice (parallel replicates, late Holocene)	37	17	2.2
NGRIP (bag replicates of gas cut, Holocene)	27	13	2.3

unpyrolysed CH_4 and Kr on the target beams m/z 2 and 3 when only a basic chromatographic separation is used after the conversion step (Bock et al., 2013). Based on that, we assess in the following the origin and influence of peaks showing up after the CH_4-derived H_2 peak when a cooled PLOT column is used for separation, subsequently referred to as post-peaks (Fig. 2). Implementation of the cooled 2nd GC revealed additional substances causing signals in the mass spectrometer either due to a direct effect or via the production of a third substance from the eluting substance plus background. The latter effect, occurring in the ion source, is named in situ production.

For pure CH_4 in He injections, signals on m/z 12, 14, 15, 16, 17, 18, 20, 28, 32, 40 and 44 are found for the respective focussing of the mass spectrometer (data not shown). In Table 2 we list all species measured with the 2014 set-up (Fig. 1 and Table 1). From the measurements of the different species at different focus settings, we conclude that the main components are N_2 and CO measured ca. 9 and 20 s after the H_2 peak maximum, respectively (Fig. 2). Furthermore, Ar, O_2, unpyrolysed CH_4 and Kr elute from the 2nd GC and are baseline-separated from our target H_2 (Fig. 2 and Table 2). H_2O, N_2O and CO_2 cannot pass the cold trap between the pyrolysis oven and T7 but are visible when the mass spectrometer is focussed to their typical m/z settings. Therefore, these gases must be produced from eluting peaks plus background gases present in the ion source. It is evident that H_2 peaks produce a signal on m/z 18 (and 17), with the latter peaking shortly (ca. 0.5 s) after the H_2 peak maximum. We propose that water is produced in situ within the ion source from oxygen-containing species already present in the ion source (CO, CO_2, O_2, H_2O). Tests indicate that the changes in the history of H_2O-generating background levels in the mass spectrometer can significantly alter the isotopic signature of pure (rectangular) H_2 peaks. Specifically, we find decreased δD(H_2) values for higher water levels (generated in the ion source). Performing the same measurements at lower electron voltages (from 90 to 70 eV) reduces the effect and is generally recommended for δD(H_2) analysis due to the formation of $^4He^{2+}$ at voltages >79 eV (Denifl et al., 2002) (and comments by W. Brand in the Isogeochem archive, 2002 and 2005, http://list.uvm.edu/cgi-bin/wa?A0=ISOGEOCHEM).

In any case, it is possible to create and maintain stable conditions for our complete system enabling robust δD(CH_4) measurements, that is, strictly following the "identical treatment" (IT) principle of samples and references (Werner and Brand, 2001). To provide each CH_4-derived H_2 peak with identical background conditions, we stick to the previously described regular injections of either pure CH_4 in He or sample/reference air-derived CH_4 every 20 min (Bock et al., 2010a) and leave the open split inserted over the course of the day. Obviously, also pure H_2 rectangular monitoring peaks are injected on a regular schedule.

Table 4. Results of ice core samples from B34. Given depth indicates the middle of each sample. Depending on replicate shape and weight, typical samples are between 5 and 15 cm long. Gas ages are estimated from the official AICC2012 chronology (Veres et al., 2013) for the EDML core, which is located nearby. The standard deviation of Air Controlé measurements used to calibrate the sample is given in the column named 1σ. Samples with a weight < 220 g correspond to a methane amount comparable to samples from the glacial with lowest CH_4 concentration of around 350 ppb.

Middle depth (m)	Gas age (a BP AICC2012)	Measurement date (Day Month Year)	δD(CH_4) (‰)	1σ (‰)	Weight (g)
181.435	1401	20 Feb 2013	−74.8	0.9	219.6
181.553	1402	22 Feb 2013	−75.6	0.9	200.4
181.935	1408	21 Feb 2013	−76.7	0.9	199.4
181.935	1408	12 Mar 2013	−75.0	0.9	200.4
183.065	1424	2 Nov 2011	−79.0	1.9	202.3
183.065	1424	3 Nov 2011	−73.6	1.9	209.7
183.128	1425	8 Nov 2011	−74.1	2.6	206.5
183.190	1426	15 Feb 2012	−76.2	2.7	316.7
183.190	1426	3 Nov 2011	−76.6	1.9	202.2
183.315	1428	7 Mar 2012	−77.1	1.6	261.3
183.315	1428	16 Feb 2012	−79.2	2.7	210.4
183.445	1429	1 Nov 2011	−75.5	1.9	377.0
183.445	1429	22 Feb 2012	−78.8	3.3	264.4
183.570	1431	8 Dec 2011	−77.2	2.1	312.6
183.695	1433	31 Oct 2011	−78.4	1.9	394.3
183.825	1435	30 Sep 2011	−78.8	1.2	349.1
183.825	1435	28 Sep 2011	−74.6	1.2	376.5
183.945	1437	10 Feb 2012	−73.7	2.7	318.5
184.150	1440	11 Sep 2013	−76.8	1.2	254.6
184.150	1440	18 Jul 2013	−75.5	1.4	293.3
184.150	1440	20 Aug 2013	−73.6	1.8	298.8
184.150	1440	13 Sep 2013	−73.3	1.2	267.6
184.380	1443	5 Aug 2013	−75.1	1.7	232.2
184.380	1443	26 Jul 2013	−71.6	1.4	224.4
184.550	1446	12 Jul 2013	−70.9	0.9	250.6
184.550	1446	19 Aug 2013	−72.2	1.8	259.0
184.550	1446	10 Apr 2014	−72.5	1.1	233.9
184.550	1446	14 Apr 2014	−72.7	1.1	245.7
184.730	1449	13 Jun 2013	−76.3	1.2	211.6
184.730	1449	7 Jun 2013	−75.2	1.2	257.0
184.730	1449	11 Apr 2014	−71.0	1.1	253.2
184.730	1449	15 Apr 2014	−69.4	1.1	237.8
184.910	1451	18 Jun 2013	−70.9	1.1	251.5
184.910	1451	6 Jun 2013	−74.2	1.2	239.8
185.190	1455	18 Jul 2011	−74.5	1.2	223.8
185.190	1455	18 Jul 2011	−77.5	1.2	212.9
185.338	1458	15 Jul 2011	−73.9	1.2	446.0
185.338	1458	15 Jul 2011	−73.3	1.2	427.6
185.500	1460	26 Apr 2011	−75.3	0.4	427.0
186.985	1481	19 Mar 2013	−72.3	0.9	408.6
187.133	1483	19 Feb 2013	−71.6	0.9	310.0
187.420	1487	24 Oct 2012	−70.9	1.9	347.4
187.420	1487	23 Oct 2012	−74.2	1.9	340.7
190.475	1528	31 May 2013	−68.7	1.2	261.7
190.475	1528	4 Jun 2013	−68.0	1.2	251.4
190.565	1529	30 May 2013	−70.1	1.2	262.3
190.565	1529	22 May 2013	−71.3	1.2	250.7
190.655	1530	17 May 2013	−76.9	1.1	264.4
190.775	1532	5 Jun 2013	−80.2	1.2	205.1
190.775	1532	15 May 2013	−73.9	1.0	229.4
190.775	1532	8 May 2013	−72.9	0.5	245.1

In the following we will discuss the accuracy of our new system and its consistency with previous versions of our δD(CH_4) analysis (Table 1). As presented in Table 2, the first post-peak (mostly N_2) is due to trapped background nitrogen in the He carrier gas stream. Assuming constant background (leak rate) conditions over the course of a day, any effect will cancel out by adhering to the IT principle of samples and references (Werner and Brand, 2001). The second post-peak (CO) is produced as a side product of CH_4 pyrolysis. In our previous report (Bock et al., 2010a), we showed that within the precision of that time, neither changes in CH_4 concentration nor sample volume influence δD(CH_4) for our extraction/conversion line. Hence, the IT principle is also valid here, as we match the peak sizes (i.e. methane amount) for samples and references. On the contrary, differences may occur in systems with or without post-conversion GC separation caused by unpyrolysed CH_4 and Kr. Results for Saphir 3 (Table 3), an artificial air sample containing no krypton, which was re-measured with a -5.8 ‰ offset and with a combined error of 3.5 ‰ (the square root of the sum of the squared standard deviations of samples and reference measurements) using the system with only basic 2nd GC separation (blue in Fig. 1 and Table 1), may indicate such an effect. Although this offset is still within 2σ of the error, we speculate that this is related to the Kr effect for the older measurements without post pyrolysis GC separation. In the discussion version of this contribution, we demonstrate that Kr produces a positive signal on $m/z\,2$ and a negative signal on $m/z\,3$ (Bock et al., 2013). The effect for Saphir is maximal as we reference this gas mixture to a standard containing recent Kr and CH_4 concentrations (Air Controlé) (see also Schmitt et al., 2013). Using a 2nd GC separation, separating Kr from the CH_4-derived H_2 peak as in the latest version of our method, a Kr effect is completely avoided.

Generally, we have found our system to be remarkably stable over the past several years, despite the implemented changes (Table 1 and Fig. 1). Table 3 summarizes our results and shows no significant differences for Alert, Boulder, NAT-332, Dome6 or ice samples when comparing the different stages of our system.

Using the 2014 set-up, Alert, our primary standard and anchor with respect to VSMOW, has been re-measured with a difference of $+0.8$ ‰ compared to Bock et al. (2010a), which is not significant with respect to the measurement errors. We decided not to shift our scale based on these six measurements.

3.2 Precision and sample size

In this section we describe the improvements concerning precision and sample size due to pre- and post-pyrolysis trapping of methane and hydrogen, respectively. In our old system (without pre&postPT) a typical sample (up to 500 g of polar ice with CH_4 concentrations between 350 and 700 ppb) showed peak heights of the major beam between 0.6 and 1.3 nA (for ice core samples presented in Bock et al., 2010b). While peak areas are still in the same range for identical amounts of CH_4, major peak heights are increased roughly fourfold due to postPT.

In Table 4 and Fig. 4, we present 51 ice core samples (see Sect. 3.3) of a core dry drilled next to the EPICA

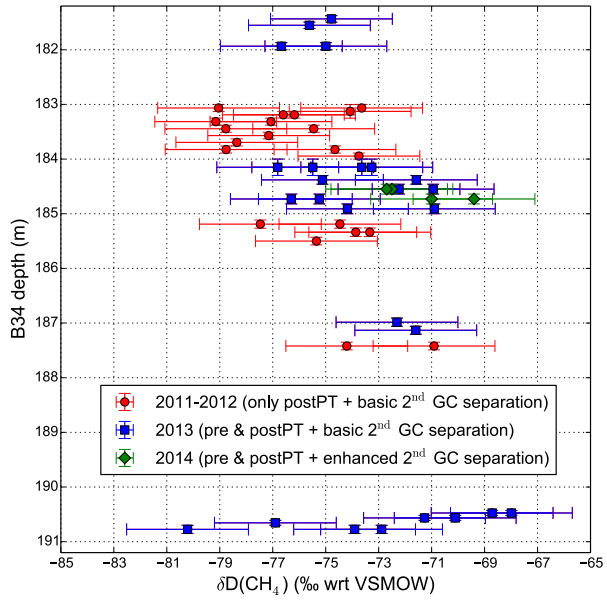

Figure 4. δD(CH$_4$) of B34 ice core samples measured during the years 2011 to 2014 (using the different set-ups shown in Table 1 and Fig. 1) on a depth scale. Error bars represent the pooled standard deviation of B34 replicates (2.3 ‰) for δD(CH$_4$) and the total depth range of each individual sample. The 10 m depth interval presented here corresponds to an age range of approximately 150 a; accordingly, a depth change of 1 m represents a nominal age increase of about 15 a, which is significantly smaller than the width of the age distribution of the bubbles in the ice.

(European Project for Ice Coring in Antarctica) drill site in Dronning Maud Land, Antarctica (EDML, 75°0.15′ S, 00°4.104′ E, 2892 m a.s.l.), called "B34". For B34 ice core sample sizes between 200 and 450 g (with a CH$_4$ concentration of roughly 640 ppb), we now obtain peak heights between 1.5 and 4.3 nA. To mimic low glacial CH$_4$ concentrations, only 200–220 g samples of B34 ice (equivalent to 350–400 g with 350 ppb CH$_4$ as found for the Last Glacial Maximum) were used and are listed in Table 4.

Table 3 summarizes our isotope results for air standards and ice samples. It is clear that precision of the new set-up has improved as indicated by smaller standard deviations of air standards (1.8 ‰ or better) and pooled standard deviations of ice core samples (2.3 ‰ or better).

Note that the precision is comparable for small and large B34 samples (Table 4). Based on the pooled standard deviation of B34 samples from the same depths measured between 2011 and 2014, we estimate that our system's precision for ice samples is around 2.3 ‰. Note that with this method, δD(CH$_4$) of present-day tropospheric air can be measured with a precision of better than 1 ‰ on 18–40 mL (STP) samples (Table 3).

Most of the gain in precision of the improved system is due to pre&postPT, and only a small fraction can be attributed to our data processing routine. We assessed this by re-evaluating the standard measurements of our data set presented in Bock et al. (2010b) with the new Python routine described in the Appendix. The standard deviation of all Air Controlé measurements using the new tool is 2.5 ‰ compared to 2.8 ‰ using the old procedure. Note, however, that even the smallest peaks of the old batch were larger by a factor of 1.6 compared to the peaks that can now be measured with comparable precision using pre&postPT. Furthermore, we acquired several runs of pure CH$_4$ in He injections of varying methane amounts with and without pre&postPT as a second measure of the gain in precision. For the old system we obtained a standard deviation of 2.0 ‰ for peak areas between 1.8 and 13.3 nA. The smallest peaks between 1.8 and 3.0 nA could be measured with a precision of 2.6 ‰. After introducing pre&postPT, we are able to achieve a precision of 1.6 ‰ for even smaller peaks between 1.3 and 1.7 nAs. As seen for the re-evaluated Air Controlé measurements, the gain is smaller for larger peaks as indicated by a standard deviation of 1.4 ‰ for peak areas between 1.3 and 6.9 nAs. We conclude that the new data processing tool presented here represents an efficient and robust way to handle time drifts and signal dependency in one step, but the main benefit with respect to precision is attributed to the implementation of pre- and post-pyrolysis trapping of methane and hydrogen, respectively.

3.3 First results

B34 ice core samples described in the last section have been analysed thoroughly using the different set-ups. No B34-specific gas age scale has been established; however, due to its vicinity to EDML, we make use of the Antarctic Ice Core Chronology 2012 (AICC2012) (Veres et al., 2013) to derive gas age estimates: on the EDML scale the depth range 181–191 mbs corresponds to an age of the occluded air of 1401–1532 a BP (Table 4). Note that in ice cores, the extracted air is integrated over a large number of individual air bubbles in the ice, which have somewhat different gas ages due to the bubble close-off process in the firn column. Accordingly, ice cores provide only a low-pass filtered signal of the atmospheric concentration. Using the firn model described by Spahni et al. (2003), we calculated the age distribution for EDML in the Holocene, representing the distribution of the gas age in each bubble: the peak in the age distribution is at 33 a and the width at half-maximum is 67 a. Figure 4 shows δD(CH$_4$) measured on B34 ice samples on a depth scale. The same data are also presented in Table 4, which additionally shows gas age, the measurement date and the weight of samples. Overall, we are confident that the described system was stable in terms of accuracy over the past few years, and the pooled standard deviation of all replicates ($N = 41$, identical depths = 17) is 2.3 ‰.

Along with our measurements on standard air tanks, the ice sample data for all set-ups agree within the overall scatter of all data. Despite the fact that the samples have been measured with three different measurement systems and over a time span of several years, all samples agree within 2σ for any given depth interval and most samples agree within 1σ, showing that they are statistically identical. Despite this statistical agreement there seems to be the tendency of samples taken at exactly the same depth to agree better than samples that have been cut from adjacent ice, which, due to the slow bubble enclosure process, should be regarded as replicates as well. Moreover, there seems to be some variability in the average δD(CH_4) value on the metre depth scale, which is unexpected given the wide age distribution of the air bubbles, which quite effectively smoothes out multi-annual atmospheric variability. Whether this is due to an incomplete understanding of the bubble close-off process in this core, reflects limited potential in situ CH_4 formation (Rhodes et al., 2013) or remains just statistical coincidence requires further dedicated studies in the future using an identical measurement system.

Mean values for WAIS (Antarctica) and B30 (Greenland) from similar (pre-industrial) time periods (around 410 and 670 a BP, respectively) are -73.0 and -91.5 ‰. This difference of 18.5 ‰ with a combined error of 1.9 ‰ (determined as above) can be largely explained by the expected interpolar difference in δD(CH_4), which can be explained by the geographical distribution of CH_4 sources with different δD(CH_4) signature in combination with the inter-hemispheric air mass exchange and the lifetime of CH_4 of the order of 8–10 years. It is beyond the scope of this article to discuss the biogeochemical implications of this finding, but we note that the interpolar difference derived from our measurements is in line with earlier work (Sowers, 2010; Quay et al., 1999).

4 Conclusions

We presented pre- and post-pyrolysis trapping of methane and hydrogen, respectively, combined with post-trapping GC separation on a cooled PLOT column to improve accuracy and precision and reduce sample amount in δD(CH_4) analysis of atmospheric and ice core samples. We showed that the precision for 350 g of ice (or roughly 30 mL of air) with 350 ppb of methane is approximately 2.3 ‰. This corresponds to recent tropospheric air samples (roughly 1900 ppb CH_4) of about 6 mL (STP) or about 500 pmol of pure CH_4. In contrast, 30 mL (STP) samples with recent tropospheric CH_4 concentration can be determined with a precision of better than 1 ‰. Compared to our old set-up (Bock et al., 2010a), this translates into improvement factors for sample size (350 g)/(500 g) and precision (2.3 ‰)/(3.4 ‰) of 0.7.

We note, however, that the high standard in accuracy and precision for such small samples is achieved at the cost of sample throughput; typically we can measure eight standards in addition to at most two ice core samples or four atmospheric samples a day.

We showed that the accuracy of systems without pre&postPT and subsequent chromatographic separation can be potentially biased depending on pyrolysis efficiency and varying methane/krypton ratios in samples and the reference. However, for atmospheric samples (ice and tropospheric air samples), the updated method did not measurably change in terms of accuracy of δD(CH_4) values compared to our initial set-up described in Bock et al. (2010a).

We propose that water produced in situ in the ion source of the mass spectrometer from hydrogen plus oxygen-containing background species may be an important factor affecting precision and accuracy of δD measurements. In our case we take advantage of simple chromatograms and regular injections to ensure identical background levels for each sample or reference peak.

Appendix A: Correction for system drifts and signal dependency (linearity)

In order to calibrate samples measured on any isotope system, it is essential to compare samples to standard measurements that are sufficiently stable in time and match the sample size, or to correct for any drift and signal dependency. As amount effects alter isotopic results simultaneously with (time) drift effects, both errors should be corrected at the same time and not consecutively. A decoupling of the corrections is only possible when standards of constant peak size are measured to monitor the time trends only. Effects of signal dependency can be assessed by performing standard runs of different peak sizes; however, this is quite time-consuming. Hence, we present an approach which allows for simultaneous corrections of system drifts and signal dependency effects. For optimum conditions we choose size matching and bracketing standards for individual samples and pool standards measured over several days (assuming constant signal dependency over this time period) to cover the samples' size range. To correct for both signal dependency and drift effects, we use the following approach.

Any measured isotope value δX^{meas} is composed of the true value δX^{true}, any signal dependency, which is a function of peak area, A, and a drift correction, which is a function of time, t:

$$\delta X^{\text{true}} = \delta X^{\text{meas}} - f^{\text{lin}}(A) - f^{\text{drift}}(t). \tag{A1}$$

In the following, signal dependency is characterized by a polynomial of order N:

$$f^{\text{lin}}(A) = \sum_{n=1}^{N} x_n A^n. \tag{A2}$$

System drift is decomposed into two additive terms:

$$f^{\text{drift}}(t) = f_1^{\text{drift}}(t) + f_2^{\text{drift}}(t). \tag{A3}$$

The first term is a drift over the course of a day, which is fitted to a polynomial of order M:

$$f_1^{\text{drift}}(t) = \sum_{m=1}^{M} y_m t^m \Theta(t - [\overline{t_i} - \Delta t])\Theta([\overline{t_i} + \Delta t] - t), \tag{A4}$$

which is a function of time t. Here, t_i represents the time during day i at which the current sample was measured. Thus, $\overline{t_i}$ describes the mean measurement time of all samples measured during one day. Since temporal system drifts typically occur on timescales of weeks to months, the size of the drift within a day is usually small. Accordingly, our software allows for the calculation of δD(CH_4) values with or without a diurnal drift correction (the latter is usually our preferred setting). The Theta function, Θ, is zero if its argument is < 0 and one if its argument is > 0. This efficiently allows for the determination of the drift for each single measurement day in the program code. To discriminate between two consecutive laboratory days, Δt is defined as 0.4 days. The number of standard data points for each day should be greater than or equal to M.

The second term represents the drift of the reference values between days. The mean isotopic reference signatures of all days are assumed to change in a stepwise linear fashion:

$$f_2^{\text{drift}}(t) = \sum_{i=1}^{L} (m_i t + n_i)\Theta(\overline{t_i} - t)\Theta(t - \overline{t_{i-1}}), \tag{A5}$$

where m_i quantifies the slope and n_i the intersection with the ordinate on measuring day i, and L is the number of all measurement days.

Slope and intersect for each day i are calculated with respect to the previous day $i-1$.

$$m_i = \frac{\overline{t_i} - \overline{t_{i-1}}}{\left[\overline{\delta X_i^{\text{meas}} - f^{\text{lin}}(A_i)}\right] - \left[\overline{\delta X_{i-1}^{\text{meas}} - f^{\text{lin}}(A_{i-1})}\right]} \tag{A6}$$

$$n_i = \left[\overline{\delta X_i^{\text{meas}} - f^{\text{lin}}(A_i)}\right] - m_i \overline{t_i}. \tag{A7}$$

Influences of signal dependency have to be corrected for before calculating the mean standard isotopic signal of each day.

We can express all quantities given in Eq. (A1) as functions of peak area, A, and isotopic signature δX^{meas} at each point measured at time, t. The true value of the standard δX^{true} is known. Thus, Eq. (A1) can be used to fit all measured data points. The fit parameters determine both the signal dependency and the drifts during and between days and are found by minimizing the standard deviation of all drift and signal dependency corrected standard values. The fitted parameters are then used to ultimately calibrate the samples.

Our routine is written in Python (www.python.org). The actual optimization uses the function scipy.optimize.fmin(). Figure 3a and b are produced by our routine and show uncalibrated and calibrated data, respectively. Each subfigure shows signal dependency in the left panel and time drift in the right panel (using the same data in the two panels).

Acknowledgements. Financial support for this study was provided in part by Schweizerischer Nationalfonds (SNF project primeMETHANE) and the European Research Council advanced grant MATRICs. We are grateful for B34 standard ice core samples provided by the Alfred-Wegener-Institut Helmholtz-Zentrum für Polar- und Meeresforschung (AWI). Many thanks to Willi Brand, Ingeborg Levin, Thomas Röckmann, Peter Sperlich and Cordelia Veidt for their help in evaluating lab offsets relative to the VSMOW scale. We thank Hinrich Schaefer, who had the insight to suggest additional important interferences, as well as Todd Sowers and another anonymous referee for the helpful reviews.

Edited by: F. Keppler

References

Bergamaschi, P., Schupp, M., and Harris, G. W.: High-precision direct measurements of $^{13}CH_4/^{12}CH_4$ and $^{12}CH_3D/^{12}CH_4$ ratios in atmospheric methane sources by means of a long-path tunable diode laser absorption spectrometer, Appl. Optics, 33, 7704–7716, 1994.

Bergamaschi, P., Bräunlich, M., Marik, T., and Brenninkmeijer, C. A. M.: Measurements of the carbon and hydrogen isotopes of atmospheric methane at Izaña, Tenerife: Seasonal cycles and synoptic-scale variations, J. Geophys. Res., 105, 14531–14546, doi:10.1029/1999JD901176, 2000.

Bock, M., Schmitt, J., Behrens, M., Möller, L., Schneider, R., Sapart, C., and Fischer, H.: A gas chromatography/pyrolysis/isotope ratio mass spectrometry system for high-precision δD measurements of atmospheric methane extracted from ice cores, Rapid Commun. Mass Sp., 24, 621–633, doi:10.1002/rcm.4429, 2010a.

Bock, M., Schmitt, J., Möller, L., Spahni, R., Blunier, T., and Fischer, H.: Hydrogen Isotopes Preclude Marine Hydrate CH_4 Emissions at the Onset of Dansgaard-Oeschger Events, Science, 328, 1686–1689, 2010b.

Bock, M., Schmitt, J., Beck, J., Schneider, R., and Fischer, H.: Improving accuracy and precision of ice core δD(CH_4) analyses using methane pre- and hydrogen post-pyrolysis trapping and subsequent chromatographic separation, Atmos. Meas. Tech. Discuss., 6, 11279–11307, doi:10.5194/amtd-6-11279-2013, 2013.

Brass, M. and Röckmann, T.: Continuous-flow isotope ratio mass spectrometry method for carbon and hydrogen isotope measurements on atmospheric methane, Atmos. Meas. Tech., 3, 1707–1721, doi:10.5194/amt-3-1707-2010, 2010.

Bräunlich, M., Aballain, O., Marik, T., Jaeckel, P., Brenninkmeijer, C. A. M., Chappellaz, J., Barnola, J.-M., Mulvaney, R., and Sturges, W. T.: Changes in the global atmospheric methane budget over the last decades inferred from 13C and D isotopic analysis of Antarctic firn air, J. Geophys. Res., 106, 20465–20481, doi:10.1029/2001JD900190, 2001.

Clark, P. U., Dyke, A. S., Shakun, J. D., Carlson, A. E., Clark, J., Wohlfarth, B., Mitrovica, J. X., Hostetler, S. W., and McCabe, A. M.: The Last Glacial Maximum, Science, 325, 710–714, doi:10.1126/science.1172873, 2009.

Denifl, S., Gstir, B., Hanel, G., Feketeova, L., Matejcik, S., Becker, K., Stamatovic, A., Scheier, P., and Märk, T. D.: Multiple ionization of helium and krypton by electron impact close to threshold: appearance energies and Wannier exponents, J. Phys. B, 35, 4685, doi:10.1088/0953-4075/35/22/310, 2002.

Dlugokencky, E. J., Steele, L. P., Lang, P. M., and Masarie, K. A.: Atmospheric methane at Mauna Loa and Barrow observatories: Presentation and analysis of in situ measurements, J. Geophys. Res., 100, 23103–23113, doi:10.1029/95JD02460, 1995.

Ferretti, D. F., Miller, J. B., White, J. W. C., Etheridge, D. M., Lassey, K. R., Lowe, D. C., Meure, C. M. M., Dreier, M. F., Trudinger, C. M., van Ommen, T. D., and Langenfelds, R. L.: Unexpected Changes to the Global Methane Budget over the Past 2000 Years, Science, 309, 1714–1717, 2005.

Fischer, H., Behrens, M., Bock, M., Richter, U., Schmitt, J., Loulergue, L., Chappellaz, J., Spahni, R., Blunier, T., Leuenberger, M., and Stocker, T. F.: Changing boreal methane sources and constant biomass burning during the last termination., Nature, 452, 864–867, doi:10.1038/nature06825, 2008.

Intergovernmental Panel on Climate Change: Climate Change 2007 – The Physical Science Basis: Working Group I Contribution to the Fourth Assessment Report of the IPCC (Climate Change 2007), Cambridge University Press, available at: http://www.worldcat.org/isbn/0521705967 (last access: 30 June 2014), 2007.

Kennett, J. P., Cannariato, K. G., Hendy, I. L., and Behl, R. J.: Methane Hydrates in Quaternary Climate Change: The Clathrate Gun Hypothesis, AGU Special Publication, 2003.

Kirschke, S., Bousquet, P., Ciais, P., Saunois, M., Canadell, J. G., Dlugokencky, E. J., Bergamaschi, P., Bergmann, D., Blake, D. R., Bruhwiler, L., Cameron-Smith, P., Castaldi, S., Chevallier, F., Feng, L., Fraser, A., Heimann, M., Hodson, E. L., Houweling, S., Josse, B., Fraser, P. J., Krummel, P. B., Lamarque, J.-F., Langenfelds, R. L., Le Quere, C., Naik, V., O'Doherty, S., Palmer, P. I., Pison, I., Plummer, D., Poulter, B., Prinn, R. G., Rigby, M., Ringeval, B., Santini, M., Schmidt, M., Shindell, D. T., Simpson, I. J., Spahni, R., Steele, L. P., Strode, S. A., Sudo, K., Szopa, S., van der Werf, G. R., Voulgarakis, A., van Weele, M., Weiss, R. F., Williams, J. E., and Zeng, G.: Three decades of global methane sources and sinks, Nat. Geosci., 6, 813–823, doi:10.1038/ngeo1955, 2013.

Loulergue, L., Schilt, A., Spahni, R., Masson-Delmotte, V., Blunier, T., Lemieux, B., Barnola, J.-M., Raynaud, D., Stocker, T. F., and Chappellaz, J.: Orbital and millennial-scale features of atmospheric CH_4 over the past 800,000 years, Nature, 453, 383–386, doi:10.1038/nature06950, 2008.

Marik, T.: Atmospheric δ^{13}C and δD Measurements to Balance the Global Methane Budget, Ph.D. thesis, University of Heidelberg, 1998.

Meier-Augenstein, W.: Applied gas chromatography coupled to isotope ratio mass spectrometry, J. Chromatogr. A, 842, 351–371, 1999.

Meier-Augenstein, W., Kemp, H. F., and Lock, C. M.: N_2: a potential pitfall for bulk ^{2}H isotope analysis of explosives and other nitrogen-rich compounds by continuous-flow isotope-ratio mass spectrometry, Rapid Commun. Mass Sp., 23, 2011–2016, doi:10.1002/rcm.4112, 2009.

Mischler, J. A., Sowers, T. A., Alley, R. B., Battle, M., McConnell, J. R., Mitchell, L., Popp, T., Sofen, E., and Spencer, M. K.: Carbon and hydrogen isotopic composition of methane over the last 1000 years, Global Biogeochem. Cy., 23, GB4024, doi:10.1029/2009GB003460, 2009.

Mitchell, L. E., Brook, E. J., Sowers, T., McConnell, J. R., and Taylor, K.: Multidecadal variability of atmospheric methane, 1000–1800 C.E., J. Geophys. Res., 116, G02007, doi:10.1029/2010JG001441, 2011.

Möller, L., Sowers, T., Bock, M., Spahni, R., Behrens, M., Schmitt, J., Miller, H., and Fischer, H.: Independent variations of CH_4 emissions and isotopic composition over the past 160,000 years, Nat. Geosci., 6, 885–890, doi10.1038/ngeo1922, 2013.

Poss, C.: Untersuchung der Variabilität des atmosphärischen Methanhaushalts hochpolarer Breiten anhand eines regionalen Trajektorienmodells und der Messung stabiler Isotope, Ph.D. thesis, University of Heidelberg, 2003.

Potter, J. and Siemann, M. G.: A new method for determining δ^{13}C and δD simultaneously for CH_4 by gas chromatography/continuous-flow isotope-ratio mass spectrometry, Rapid Commun. Mass Sp., 18, 175–180, doi:10.1002/rcm.1311, 2004.

Quay, P., Stutsman, J., Wilbur, D., Snover, A., Dlugokencky, E., and Brown, T.: The Isotopic Composition of Atmospheric Methane, Global Biogeochem. Cy., 13, 445–461, doi:10.1029/1998GB900006, 1999.

Rhodes, R. H., Faïn, X., Stowasser, C., Blunier, T., Chappellaz, J., McConnell, J. R., Romanini, D., Mitchell, L. E., and Brook, E. J.: Continuous methane measurements from a late Holocene Greenland ice core: Atmospheric and in-situ signals, Earth Planet. Sc. Lett., 368, 9–19, doi:10.1016/j.epsl.2013.02.034, 2013.

Ricci, M. P., Merritt, D. A., Freeman, K. H., and Hayes, J.: Acquisition and processing of data for isotope-ratio-monitoring mass spectrometry, Org. Geochem., 21, 561–571, 1994.

Sapart, C. J., van der Veen, C., Vigano, I., Brass„ M., van de Wal, R. S. W., Bock, M., Fischer, H., Sowers, T., Buizert, C., Sperlich, P., Blunier, T., Behrens, M., Schmitt, J., Seth, B., and Röckmann, T.: Simultaneous stable isotope analysis of methane and nitrous oxide on ice core samples, Atmos. Meas. Tech., 4, 2607–2618, doi:10.5194/amt-4-2607-2011, 2011.

Sapart, C. J., Monteil, G., Prokopiou, M., van de Wal, R. S. W., Kaplan, J. O., Sperlich, P., Krumhardt, K. M., van der Veen, C., Houweling, S., Krol, M. C., Blunier, T., Sowers, T., Martinerie, P., Witrant, E., Dahl-Jensen, D., and Röckmann, T.: Natural and anthropogenic variations in methane sources during the past two millennia, Nature, 490, 85–88, doi:10.1038/nature11461, 2012.

Schmitt, J.: A sublimation technique for high-precision δ^{13}C on CO_2 and CO_2 mixing ratio from air trapped in deep ice cores, Ph.D. thesis, University of Bremen, 2006.

Schmitt, J., Glaser, B., and Zech, W.: Amount-dependent isotopic fractionation during compound-specific isotope analysis, Rapid Commun. Mass Sp., 17, 970–977, doi:10.1002/rcm.1009, 2003.

Schmitt, J., Seth, B., Bock, M., van der Veen, C., Möller, L., Sapart, C. J., Prokopiou, M., Sowers, T., Röckmann, T., and Fischer, H.: On the interference of Kr during carbon isotope analysis of methane using continuous-flow combustion-isotope ratio mass spectrometry, Atmos. Meas. Tech., 6, 1425–1445, doi:10.5194/amt-6-1425-2013, 2013.

Schmitt, J., Seth, B., Bock, M., and Fischer, H.: Online technique for isotope and mixing ratios of CH_4, N_2O, Xe and mixing ratios of organic trace gases on a single ice core sample, Atmos. Meas. Tech. Discuss., 7, 2017–2069, doi:10.5194/amtd-7-2017-2014, 2014.

Sowers, T.: Late Quaternary Atmospheric CH_4 Isotope Record Suggests Marine Clathrates Are Stable, Science, 311, 838–840, doi:10.1126/science.1121235, 2006.

Sowers, T.: Atmospheric methane isotope records covering the Holocene period, Quaternary Sci. Rev., 29, 213–221, 2010.

Spahni, R., Schwander, J., Flückiger, J., Stauffer, B., Chappellaz, J., and Raynaud, D.: The attenuation of fast atmospheric CH_4 variations recorded in polar ice cores, Geophys. Res. Lett., 30, 1571, doi:10.1029/2003GL017093, 2003.

Veres, D., Bazin, L., Landais, A., Toyé Mahamadou Kele, H., Lemieux-Dudon, B., Parrenin, F., Martinerie, P., Blayo, E., Blunier, T., Capron, E., Chappellaz, J., Rasmussen, S. O., Severi, M., Svensson, A., Vinther, B., and Wolff, E. W.: The Antarctic ice core chronology (AICC2012): an optimized multi-parameter and multi-site dating approach for the last 120 thousand years, Clim. Past, 9, 1733–1748, doi:10.5194/cp-9-1733-2013, 2013.

Werner, R. A. and Brand, W. A.: Referencing strategies and techniques in stable isotope ratio analysis, Rapid Commun. Mass Sp., 15, 501–519, doi:10.1002/rcm.258, 2001.